

## SHAPES OF RANDOM CLOSED SETS

IVAN SAXL AND PETR PONÍŽIL

ABSTRAKT. Abstract. The shape properties of Voronoi polytopes generated by various point processes are examined and discussed.

Абстракт. Свойства формы областей Дирихле (Вороного) генерированных различными точечными процессами исследованы и обсуждены.

## 1. INTRODUCTION

Random tessellations are useful stochastic models of natural space filling systems (grains of polycrystal, cell of living tissues *etc.*) as well as of various products of human activities (jurisdictions, districts of administration, allotments *etc.*) Non-convexity of real tessellations is usually relatively small and convex tessellations are quite suitable and acceptable approximations. Voronoi tessellation is perhaps the most suitable model of such systems; its general definition is as follows: let  $L$  be a discrete set in  $\mathbb{R}^d$  (*e.g.* a lattice or point process) and let  $\phi$  be a positive definite quadratic form on  $\mathbb{R}^d$ . Then the Voronoi cell generated by  $x_i \in L$  is  $C_i = \{y \in \mathbb{R}^d | \phi(y - x_i) \leq \phi(y - z) \text{ for all } z \in L - \{x_i\}\}$ . The union  $\mathcal{T}$  of all cells forms a face-to-face tiling of  $\mathbb{R}^d$  with properties depending on  $L$ . It is also an affine image of another tiling whose tiles are Voronoi cells defined with respect to the standard quadratic form and another suitable discrete set  $L$ . Usually the term Voronoi cell is used only to cell defined with respect to the standard Euclidean metric [10] but it is useful to keep in the mind that the basic property of  $\mathcal{T}$ , namely tiling the space, is not lost by affine transformation (*e.g.* tiling by rhombohedra can be obtained by shearing a tiling by cubes). The general reference for Voronoi tessellations is [10], more general aspects of congruent tilings are reviewed in [7, 18] and with a particular respect to crystallography in [2]. The terminology is far from being unified as it happens frequently when one idea is developed in several distinct branches of science. Consequently, in a small review like this one, the various terms describing the same property must be at least occasionally mentioned.

A tessellation is described by the distributions of its cell characteristics. The size dependent characteristics are homogeneous functions of degree  $-k/d$  of the intensity  $\lambda = 1/\mathbf{E}v$ , *i.e.*  $\mathbf{E}\bullet(\alpha\lambda) = \alpha^{-k/d}\mathbf{E}\bullet(\lambda)$ . In  $\mathbb{R}^3$ ,  $k = 3$  for the *cell volume*  $v$ ,  $k = 2$  for the *cell surface area*  $s$  and  $k = 1$  for the *mean* (with respect to projection orientation) *cell breadth*  $w$ . Consequently, it is sufficient to examine the unit tessellations only.

The shape characteristics like *mean dihedral angle*  $\Theta$ , *randomly selected dihedral angle*  $\theta$  - *i.e.* a "typical" angle of a "typical" cell, *number of cell faces*  $n_f$  and "isoperimetric" *shape factors*  $g = 6v\sqrt{\pi/s^3}$ ,  $f = 6v/(\pi w^3)$  are independent of  $\lambda$  (the shape factors  $g = f = 1$  for a ball thus expressing the statement of the isoperimetric

2000 *Mathematics Subject Classification.* Primary 60K99.

*Key words and phrases.* Random tessellations, Voronoi polytopes, point processes.

The research was supported by Grant No. 304/00/1622 of GA ČR (I.S.) and by the Ministry of Education of the Czech Republic (contract No. VS96108-P.P.).

and Bierbach inequalities, namely that of all convex bodies of fixed volume, the ball has the smallest surface area as well as mean breadth).

Any 3D tessellation  $\mathcal{T}$  induces in section planes  $F$  a 2D tessellation  $\mathcal{T}' = \mathcal{T} \cap F$  of intensity  $\lambda' = 1/\mathbf{E}v' = \lambda\mathbf{E}w$ . The mean values of its size characteristics (*cell area*  $v'$ , *perimeter*  $s'$ ) obey the stereological relations [18]  $\mathbf{E}v' = \mathbf{E}v/\mathbf{E}w$ ,  $\mathbf{E}s' = 0.25\pi\mathbf{E}s/\mathbf{E}w$  and its shape parameters are *edge number*  $n_e = 2/(1 - \mathbf{E}\Theta'/\pi)$ , *random edge angle*  $\theta'$  and *shape factor*  $f' = 4\pi v'/s'^2$ . If the tessellation is stationary isotropic, the plane  $F$  is arbitrary, otherwise the averaging relates to a suitably defined set of planes. The properties of induced tessellations are of particular importance as *e.g.* the grain size estimation so substantial in metallurgical praxis is completely based on the inference acquired in planar sections.

A short paper on shapes of Voronoi cells covering only tessellations generated by Neyman-Scott cluster fields with rather limited cluster cardinality  $N \leq 30$  was published two years ago [14]. From that time on, the range of examined tessellations was considerably extended and generating processes  $L$  include displaced lattices of several types, hard-core and Gibbs models at one side and locally inhomogeneous Bernoulli cluster fields and mixtures on the other one. Shape properties of Voronoi cells are, in fact, properties of space filling polyhedra. That is why the first part of the paper - chapter 2 - reviews selected results concerning tiling by congruent polyhedra - an old problem started by Plato and Aristotle and constituting also the second part of the Hilbert's eighteen problem (the term tiling instead of tessellation is commonly preferred in this connection). Moreover, several such tilings are the limit cases of random tessellations generated by displaced lattices. The body of the paper reports the authors' recent results obtained by computer simulation.

## 2. POLYHEDRAL TILINGS

### 2.1. Basic types.

2.1.1. *Monohedral tilings, prototiles.* Tiling  $\mathcal{T}$ , in general, is the covering of  $\mathbb{R}^d$  by sets - *tiles* - with pairwise disjoint interiors. It is *monohedral* if each tile is congruent to a fixed set called the *prototile*, which is a homeomorphic image of the unit  $d$ -ball. All possible prototiles are neither found nor at least classified even in  $\mathbb{R}^2$ . However, if a 2D prototile is bounded it must be a convex  $n$ -gon with  $2 < n \leq 6$ . In higher dimensions, the problem is intractable and many examples of  $n$ -hedra,  $n = 4, 5, 6, 7, 8, 10, 12, 14, 18, \dots$ , tiling  $\mathbb{R}^3$  are described in the series of papers by Goldberg (*e.g.* [5, 6]). It is not even known whether the number of combinatorial (= isomorphic) prototiles is finite and whether there is an upper bound on the number of faces. Consequently, a substantial restriction of the problem is necessary.

2.1.2. *Isohedral tilings, stereohedra.* Any Euclidean motion of  $\mathbb{R}^d$  mapping each tile of  $\mathcal{T}$  onto a tile of  $\mathcal{T}$  is called the symmetry of  $\mathcal{T}$ ; the set of all symmetries of  $\mathcal{T}$  forms the discrete symmetry group  $\mathcal{S}(\mathcal{T})$ . Tilings in which  $\mathcal{S}(\mathcal{T})$  acts transitively on the tiles are called *isohedral* and their prototiles are called the *stereohedra*. Their significant property is that the number of their faces has an upper bound. By Delaunay theorem [2],  $n_f \leq 2^d(1 + a) - 1$ , where  $a$  is the number of *aspects* of the prototile (an aspect is a transitivity class of tiles with respect to the translation subgroup of  $\mathcal{S}(\mathcal{T})$  - for details see [2, 7]). In  $\mathbb{R}^3$ , the maximum number of aspects is 48, hence  $n_f \leq 390$ . However, the most complicated Voronoi cell found as yet had 38 facets [2]. The second part of the Hilbert's eighteen problem can be formulated in the above introduced terminology as follows [7]: *Does there exist an anisohedral polyhedron*

in  $\mathbb{R}^3$ ? The affirmative answer was given by Reinhardt in 1928. It is sufficient to find planar anisohedral prototiles and to take them for bases of prisms. Several examples of such planar prototiles with the corresponding references are shown in [7]; it should be noted that they need not be non-convex, the congruence can be direct and a tiling face-to-face (see below).

2.1.3. *Voronoi and lattice tilings, plesiohedra and parallelohedra.* Further restriction of the problems is achieved by considering only tilings generated by point sets via Voronoi cells; frequently also the terms *Dirichlet domains* or *plesiohedra* ( $\pi\lambda\eta\sigma\iota\omicron\varsigma$  - neighbouring) are used. Voronoi cell (with respect to the standard Euclidean metric) adjoins to any point of the generating system  $L$  all points of the embedding space lying closer to it than to any other point of the system. Voronoi tiling generated by an arbitrary point set is a *face-to-face* tiling (*i.e.*  $C_i \cap C_j$  is either  $\emptyset$  or a common face of  $C_i, C_j$ ). A tiling is called *primitive* (also the terms *ordinary equilibrium state* or *normal tessellation* are used in stochastic geometry) if exactly  $d - k + 1$  adjacent parallelotopes meet in every its  $k$ -facet (0-facet is a vertex, 1-facet is an edge,  $(d-1)$ -facet is a face). Voronoi [20] has shown that the necessary and sufficient condition of primitivity is that this rule might hold for vertices, *i.e.* just  $(d + 1)$  cells meet in each vertex. The numbers of  $k$ -facets of primitive prototiles are not independent; *e.g.* the number of vertices  $n_v = 2(n_f - 2)$  and the number of edges  $n_e = 3(n_f - 2)$  in  $\mathbb{R}^3$ . All random tessellations examined in chapters 3 and 4 are primitive and it is sufficient to consider only the number of their faces  $n_f$ .

Voronoi tilings generated by translation point lattices and called *lattice tilings* are perhaps the best analysed subclass of isohedral tilings; their prototiles are called *parallelohedra*. Voronoi [20] found the upper bound of the number of vertices for parallelohedra  $n_v \leq (d + 1)!$  and also the upper bound of the number of faces has been found by Minkowski [9]  $n_f \leq 2(2^d - 1)$  (two congruent sets have the same aspect if one is a translate of the other, *i.e.*  $a = 1$  in the Delaunay theorem).

The number  $N_d$  of combinatorial types of parallelohedra is limited;  $N_2 = 2$  - parallelogram and centrally symmetric hexagon,  $N_3 = 5$  - parallelotope, hexagonal prism, rhombic and elongated (eight rhombic and four hexagonal faces) dodecahedrons, tetrakaidecahedron (Fedorov [3]). Three of them are the prototiles of common cubic lattice tilings: cubic simple (cs - NaCl) - cube, cubic body-centred (cb - *e.g.* Fe, Cr, Mo, W) - tetrakaidecahedron, cubic face-centred (cf - *e.g.* Cu, Al, Ni) - rhombic dodecahedron. The prototile of the hexagonal close-packed lattice (*e.g.* Zn, Mg, Zr) is also a dodecahedron with eight rhombic and four trapezoidal faces combinatorially equivalent to the rhombic dodecahedron - see below. Tetrakaidecahedron has the maximum attainable number  $n_v = 24$  of 3-valent vertices (the number of edges meeting in a vertex of an isolated polyhedron) and also the maximum possible number of faces  $n_f = 2(2^d - 1)$  [9]. It is the only primitive of the Fedorov five basic space fillers. Rhombic dodecahedron has six 4-valent vertices and eight 3-valent vertices whereas cube with eight 3-valent vertices is the least primitive of them.

2.2. **Packing, covering and extremum problems.** Isohedral tilings are closely connected with packings and coverings problems, namely in the selection of the densest packing (the packing density  $\delta_K \leq 1$ , which is intuitively the ratio of the sum of the volumes of the packed bodies  $K$  to the volume of the covered space, is maximum) and of the thinnest covering (the analogically defined covering density  $\vartheta_K \geq 1$  - the ratio of the sum of the volumes of the covering bodies  $K$  to the volume of the covered space, is minimum) [4]. Packing and covering densities of monohedral

tiles equal 1, but the to packing and covering densities of spheres inscribed and circumscribed to particular tiles attract a considerable attention.

In the planar case, the closest packing of circles is that one of circles inscribed to the tiling by regular hexagons ( $\delta_K = \pi/\sqrt{12} = 0.9069$ ) and the thinnest covering is that one of the circles circumscribed to the same hexagons ( $\vartheta_K = 2\pi/\sqrt{27} = 1.209$ ). The hexagonal tiles are Voronoi cells of the circle centres and are also the solution of another extremum problem: to find a it thinnest tiling, namely that one of minimum perimeter at a given (unit, say) area. Thus the tiling by regular hexagons solves the all three extremum problems in  $\mathbb{R}^2$ . A direct generalization of this idea to higher dimensions is straightforward, namely we can look for tilings with the smallest size characteristics like surface area, mean breadth *etc.*, or in other words, for the thinnest tilings with respect to  $w, s$  *etc.* The values of the corresponding characteristics of a  $d$ -ball are the lower bounds due to already mentioned isoperimetric inequality and its generalizations and it is therefore reasonable to introduce shape parameters of the type introduced in chapter 1, namely normalized with respect to the values appropriate for  $d$ -balls.

In  $\mathbb{R}^3$ , a different situation is encountered. Replacing the circles in the densest hexagonal packing by spheres of the same radius, an elementary layer A of a three dimensional packing is formed. The sphere centres may be then considered to be the nodes of a  $\{111\}$  plane of the cubic face-centred lattice (cf). Shifting the layers subsequently by  $\frac{1}{2} \langle 1, -1, 0 \rangle$  the layers B, C and again A are formed and the whole half-space is filled by the stacking ABCABC...; similarly its complement is formed by shifts in the opposite direction. The Voronoi tiles of the sphere centres are rhombic dodecahedrons, the packing density is  $\delta_K = \pi/\sqrt{18}$ . That this is just the densest sphere packing was conjectured by Kepler or perhaps a few years before by T. Harriot (Sir Walter Raleigh's mathematical assistant). Ferguson and Hales claim to prove Kepler conjecture in 1998 by a sophisticated computational approach, but it seems that their proof is not yet generally accepted - see <http://www.math.lsa.umich.edu/~hales/>.

Tab. 1 Packing and covering densities, prototile characteristics ( $v = 1$ ).

	$\delta_K$	$\vartheta_K$	$s$	$w$
tetrakaidecahedron (cb)	0.680	1.464	5.315	1.336
rhombic dodecahedron (cf)	0.742	2.0946	5.345	1.375
cube (cs)	0.524	2.721	6	1.5

Harriot was also the first to notice that there is another packing of the same  $\delta_K$ , namely that one of the hexagonal closed packed lattice with stacking ABABAB... created by the shift sequence  $\frac{1}{2} \langle 1, -1, 0 \rangle \rightarrow \frac{1}{2} \langle -1, 1, 0 \rangle \rightarrow \frac{1}{2} \langle 1, -1, 0 \rangle \dots$ . The Voronoi tile is again a dodecahedron with 6 rhombic and 6 trapezoidal faces. The covering density is  $\vartheta_K = 2\pi/3$  in the both cases. Spheres centred in the nodes of the body-centred cubic (cb) lattice have smaller packing density (Tab. 1) but the thinnest covering  $\vartheta_K = \pi\sqrt{125}/24$ . Hence the extremum properties are split between face-centred and body-centred cubic tilings. The latter of them also solves the problem of minimum surface density. Assuming a unit tiling, the thinnest tiles must have minimum surface  $s$  - see Tab. 1. For a comparison, the spheres centred in the nodes of the cubic simple (cs) lattice have  $\delta_K = \pi/6$  only and  $\vartheta_K = \pi\sqrt{3}/2$ .

Tab. 2 Shape characteristics of basic parallelotopes.

	$n_f$	$n_e$	$n_v$	$f$	$g$	$\theta$	$\mathbf{E}\theta'$	$f'$	$\mathbf{E}v'$	CV $v'$
cb	14	36	24	0.800	0.868	$24 \times 2.186$ $12 \times 1.91$	2.0944	0.81	0.748	0.532
cf	12	24	14	0.735	0.860	2.0944	2.0944	0.81	0.727	0.565
cs	6	12	8	0.566	0.724	$\pi/2$	$\pi/2$	0.67	0.666	0.642

The numerical values of packing and covering densities as well as the size characteristics of cubic lattice tilings are shown in Tab. 1, shape properties of the corresponding tiles are in Tab. 2. As another confirmation of the tetrakaidecahedron perfection, also the values of the mean profile areas  $\mathbf{E}v'$  and of the corresponding coefficients of variation CV  $v'$  in the 2D tessellations induced by cubic lattice tilings are shown. The fraction of small profiles is small, the mean value  $\mathbf{E}v'$  is the highest and CV  $v'$  is the smallest. The shape factors are also the highest of all. Note for a comparison that a unit ball has  $s = 4.836$  and  $w = 1.241$ .

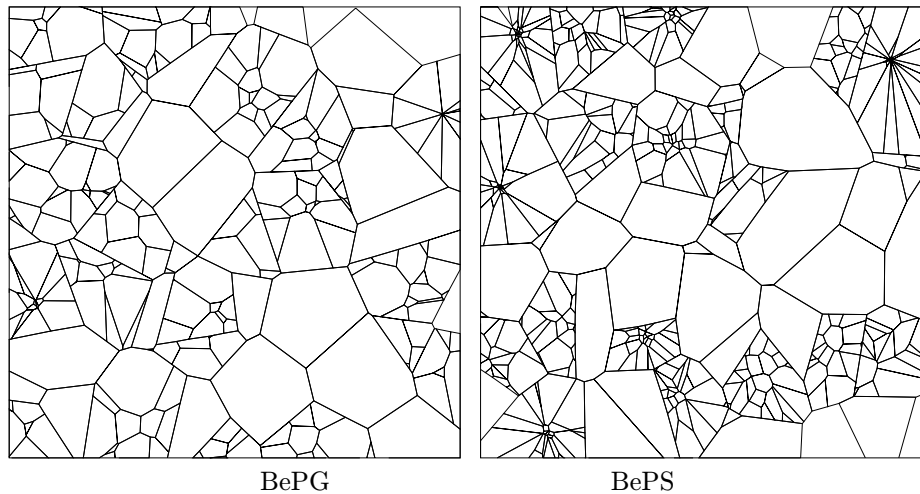
### 3. RANDOM TESSELLATIONS

**3.1. Generating point fields.** All examined point fields can be introduced in terms of the germ-grain model [18]. The germs constitute either a point lattice denoted by L or the stationary Poisson point process (PPP) denoted in this context by P, their intensities are  $\lambda_p$ . The grains implanted in the germs include several alternatives as follows (for details see [11, 12, 13, 15] and the Internet page <http://fyzika.ft.utb.cz/voronoi/>).

**3.1.1. Displaced lattices (pseudo-hard-core models).** Grains which are i.i.d. replications of randomly shifted origin (random shift vector  $\xi$ ) change the lattice of germs  $L$  (nodes  $x_i$ , say) into the Bookstein model on the lattice [19] (displaced lattice process, points  $z_i = x_i + \xi$ ). The model is widely used in physics and also in the stochastic theory of shape. The shift distribution is usually 3D normal  $N(0, \Sigma^2)$  distribution with the covariance matrix  $\Sigma^2 = a^2\mathcal{I}$ , where  $\mathcal{I}$  is the unit matrix. The process characteristics are the type of the displaced lattice and parameters of the shift distribution. The generated tessellations accomplish the bridge between the original isohedral tiling ( $a = 0$ ) and the Poisson-Voronoi tessellation (PVT) generated by the stationary Poisson point process ( $a \rightarrow \infty$ ). Above mentioned three cubic lattices have been chosen as  $L$ ; the notation is Bcs, Bcb, Bcf.

**3.1.2. Hard-core models.** If the grain is either the origin (the germ is retained) or the void set (the germ is removed) then the resulting process is either independent or dependent thinning of the germs; Bernoulli lattice process is perhaps the most familiar example of the former case. Hard-core processes like Matérn I (MI) and II (MII) type processes and SSI (simple sequential inhibition) process [18, 19] exemplify the latter case - dependent thinning of the Poisson point process (PPP) of intensity  $\lambda_0$ . The attained intensity of the thinned process  $\lambda_\bullet = p_\bullet \lambda_0$ , where  $p_\bullet$  is the Palm retaining probability of a "typical point" [18], namely the average relative gain of the thinning process;  $\bullet$  stands for I, II and SSI. The key parameters are the minimum allowable distance between points (the hard-core distance)  $D$  or, equivalently, the packing fraction  $f_p$  attained by implementing balls of diameter  $D$  into the retained germs.

**3.1.3. Cluster fields.** Grains are random point clusters  $Z$  characterized by the cluster cardinality (usually Poisson distributed)  $N_Z$  with the mean  $N$ , by the spatial arrangement (globular - G, spherical - S) of points (*daughters*) forming the cluster



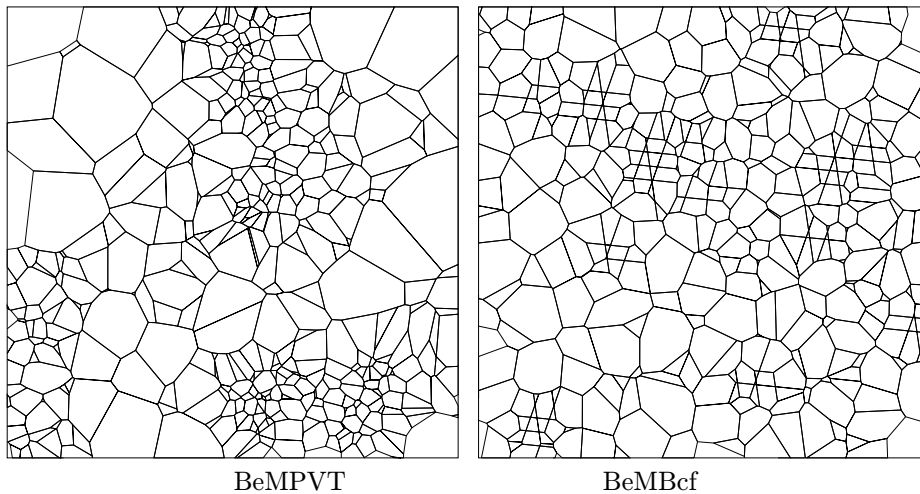
OBRÁZEK 1. Planar sections of 3D tessellations generated Bernoulli cluster fields BePG and BePS ( $N = 50, p = 0.5, \delta = 0.05$ ). The small inner cells of BePG are not perceptible in the 2D section.

and by the cluster size (e.g. by the embedding ball diameter  $D$  usually expressed as the scale independent parameter  $\delta_{\bullet} = D/\rho_p(\bullet)$ , where  $\rho_p(\bullet)$  is the mean nearest neighbour distance of the germs). *Bernoulli cluster field* [16] is a model of independent clustering: random point clusters are implanted in the parent points (which are then removed) with a probability  $0 \leq p \leq 1$ ; the resulting intensity is  $\lambda = (pN + 1 - p)\lambda_p$ . The process represents a continuous passage between PVT ( $p = 0$ ) of germs and *Neyman-Scott cluster field* ( $p = 1$ ) or germ lattice and lattice of clusters (the notation PG, PS is used for the point fields as well as for tessellations generated by them). If  $0 < p < 1$ ,  $\delta \lesssim 0.1$  and  $N$  is high, the generated tessellation is a  $(1 - p) : p$  mixture of large and only slightly corrugated parent cells and of similar cells fragmented into  $N_Z$  small cells - Fig. 1. A growth of the cluster size  $\delta$  leads to a gradual dissolution of clusters and all cluster fields approaches PPP.

3.1.4. *Mixtures*. The last examined point field is the *Bernoulli mixture process* - BeMX. Pieces of another process  $X$  of intensity  $\lambda_m$  (PPP, displaced lattices) are implanted with a probability  $0 \leq p \leq 1$  into the interior of pre-cells generated by the parent process (PPP) of intensity  $\lambda_p \ll \lambda_m$ . The resulting point process of intensity  $p\lambda_m + (1 - p)\lambda_p$  is the union of these pieces and parents of the void pre-cells. The tessellation generated by it consists of cells corresponding to the implanted process, somewhat reduced parent cells and of intermediate layers of elongated cells cutting the original faces between fragmented and unchanged pre-cells - Fig. 2.

3.2. **Basic features, inner and outer cells.** An important feature of tessellations generated by globular cluster fields are s.c. *inner cells* introduced in [12, 13]. Points of spherical clusters fragment the parent cell into more or less similar pyramidal cells nearly each of which has a base formed by a part of the parent cell boundary. Consequently, nearly each generator has a neighbour belonging to another cluster - hence the term *outer cells*.

For clusters of the G-type, the situation is similar only if the cardinality  $N_Z$  of the cluster  $Z$  is small. Starting with  $N_Z = 5$ , it may happen that all neighbours



OBRÁZEK 2. Planar sections of 3D tessellations generated by Bernoulli mixtures ( $p = 0.1$ ) with PVT ( $\lambda_m = 200\lambda_p$ ) and Bcf ( $\lambda_m = 30\lambda_p, a = 0.0005$ , *i.e.* only a slightly disturbed isohedral tiling). Pre-cells are in the both cases generated by PVT.

of a generating point are points of the same cluster; the cell generated by such a point lies completely in the interior of the parent cell and will be called the *inner cell*. The proportion  $\alpha_N$  of inner cells is a monotone increasing function of  $N$  ( $\alpha_{20} \approx 0.25$ ,  $\alpha_{30} \approx 0.4$ ,  $\alpha_{99} \approx 0.6$ ,  $\alpha_{200} \approx 0.7$ ). Nearly all properties of tessellations generated by cluster fields can be explained by using the concept of *inner* and *outer* daughters. Only occasionally small *false* inner cells are formed in PS tessellations at high values of  $N$ , namely when the distance of two parent points is comparable with the ball size  $c$  and two spherical clusters are mixed together. If the cluster size is small enough in comparison with the distances of parents the distributions of the majority of cell characteristics in tessellations generated by globular clusters are bimodal and heavy-tailed. The cells of opposite types produce very distinct modes and usually contribute to the opposite tails of the distribution in question. The type (P,L) of the parent arrangement does not influence this behaviour. In contrast to this situation, PS tessellations have unimodal distributions of cell properties.

In Bernoulli cluster fields, a particular mode in cell property distributions corresponds to the original unbroken parent cells. Consequently, the cell volume distribution is roughly bimodal with the mode ratio approximately 1: $N$  in the case of spherical clusters BePS and trimodal in the case of globular clusters BePG.

A suitable characteristic sorting the tessellations with respect to the regularity of their spatial arrangement is the coefficient of variation of the cell volume  $CV v$ . The examined tessellations have been generated by various random point fields described in the literature [18, 19]; they cover a wide range of space filling systems from isohedral tilings to highly locally inhomogeneous cases characterized by multimodal distributions of cell properties and  $0 \leq CV v \leq 8$  - see Tab. 3. However strange the Bernoulli cluster field may seem, they have been introduced by the authors in order to model grain structures of rather common low alloyed steels after certain thermal treatment.

## 4. RESULTS OF SIMULATIONS

The method of simulation is described in [12]. In [14], the results obtained for PG, PS cluster fields with  $N \leq 30$  are described. In the present paper, the range of the investigation is extended up to  $N = 200$ ,  $\delta = 0.05$ , added are Bernoulli cluster fields (at  $\delta = 0.05, p = 0.5$  unless otherwise stated) and Bernoulli mixtures (PVT & PVT at  $p = 0.1$ ). Moreover, tessellations generated by hard-core processes and displaced lattices are included. The former are represented by the Matérn type II process at the maximum attainable value of packing fraction  $f_p = 0.125$  and by SSI model at the packing fraction  $f_p \approx 0.28$ . For related results concerning Strauss model see [1]. A wide range  $0 \leq a \leq 10$  of the shift standard deviation was covered in tessellations generated by Bcs, Bcf and Bcb displaced lattices; their differences from PVT are negligible at the upper bound of  $a$ , at least as far as cell characteristics are examined. However, the attention was given mainly to a small randomization of the isohedral tilings; hence the values in tables relates to  $a = 0.05$ .

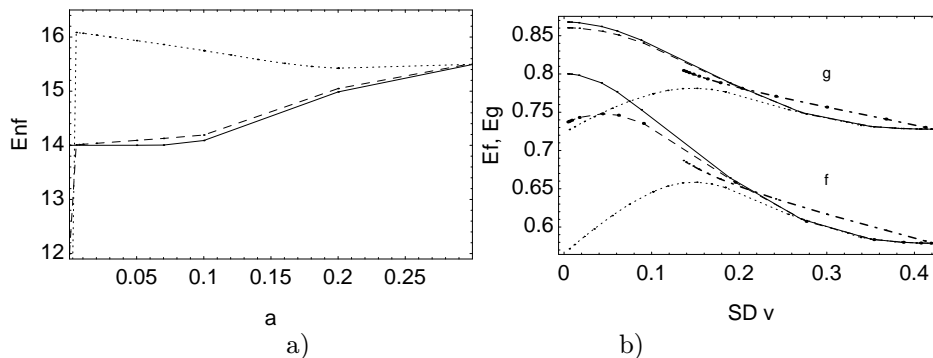
The results are presented mostly in tables. The arrows in their rows point in the direction of growing cluster cardinality  $N$  (e.g. the left arrow in the PS row of Tab. 3 shows indicates that  $n_f$  decreases with growing  $N$ ).

## 4.1. Number of faces.

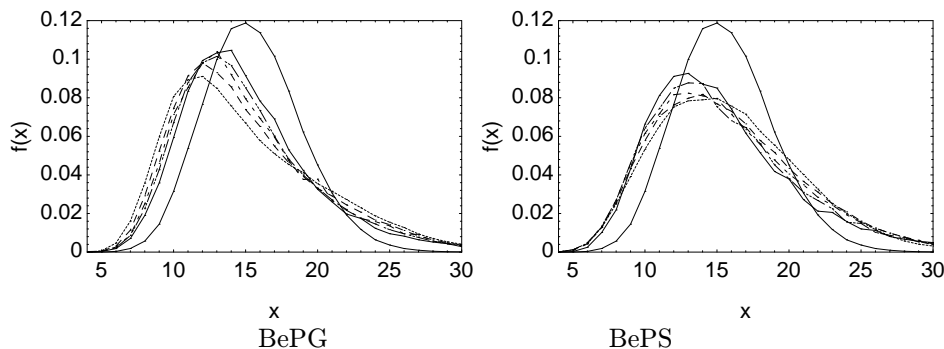
Tab. 3 Face and edge numbers, coefficient of variation CV  $v$  (the maximum values relate to the sample size  $\approx 10^6$ ).

	$N$ or $a$	var $n'$	Max $n'$	$\mathbf{E}n_f$	var $n_f$	Max $n_f$	CV $v$
Bcb	0.05	2.53	10	14.00	0.0013	15	0.043
Bcf	0.05	2.17	12	14.09	1.10	18	0.044
Bcs	0.05	2.54	13	15.93	4.68	26	0.054
SSI	-	2.41	15	15.03	3.54	25	0.136
M II	-	2.54	15	15.3	6.08	29	0.238
PVT	-	2.863	15	15.536	11.125	38	0.423
PS	30→200	2.6	15	15.2←16	25→29	58	1.10→1.28
PG	30→200	4.0	16	15.5←16	21←28	50	1.74→3.07
BeMPVT	50→200	3.5	21	15.1	18→19	86	1.55→2.97
BePS	30→99	5.5→6	27	14 - 15.5	65→100	130	2.94→5.29
BePG	30→200	5→6	27	14 - 15.5	35←40	120	3.03→7.86

4.1.1. *Hard-core and pseudo-hard-core tessellations.* Even the smallest shifts of generating points double the face number of non-primitive tiling by cubes - Fig. 3a; the tiles are truncated in all its vertices, the mode is 16 but pentakaidecahedrons and heptakaidecahedrons have only slightly lower frequencies and the pdf is fairly stable up to  $a = 0.05$ . Neither dodecahedral tiling is primitive and an abrupt change in  $n_f$  is necessary however small is  $a$ . Nevertheless, the pdf of  $n_f$  is narrow and tetrakaidecahedra and pentakaidecahedra strictly prevail at small  $a$  ( $\leq 0.05$ ). On the other hand, the primitive tetrakaidecahedral tiling is very stable, polyhedrons with  $n_f \neq 14$  are nearly completely excluded and a wider range  $13 \leq n_f \leq 17$  starts to be covered not sooner then at  $a \geq 0.1$ . Note the great differences in var  $n_f$  between Bcb, Bcf and Bcs at  $a = 0.05$  (Tab. 3). A relatively high value of var  $n'$  in Bcb is the consequence of more acute corners of the tetrakaidecahedron in the comparison with rhombic dodecahedrons (the fraction of triangular profiles is 0.03 and 0.07 in 2D tessellations induced by cf and cb tilings, respectively). The both hard-core processes are roughly comparable with the Bcs displaced lattice at  $a = 0.05$ ; the effect



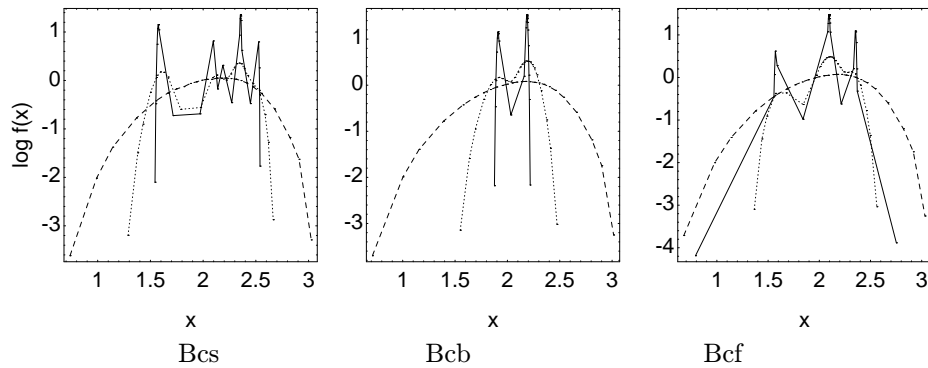
OBRÁZEK 3. a) The change in  $\mathbf{E}n_f$  in tessellations generated by displaced lattices: Bcb (full line), Bcf (dashed) and Bcs (dotted). b) The change in shape factors  $\mathbf{E}g$ ,  $\mathbf{E}f$  in tessellations generated by displaced lattices (line styles as in Fig. 3a; for a comparison the result for tessellations generated by the SSI hard-core model (dash-dotted line) is shown).



OBRÁZEK 4. Probability density functions of the cell face number  $n_f$  in BePG (a) and BePS (b) tessellations ( $p = 0.5$ ). The quasi-symmetrical pdf belongs to PVT, the mode heights increase along the sequence  $N = 30, 50, 70, 99, 200$ .

of doubled packing fraction  $f_p$  and more pronounced ordering of SSI is reflected by a lower value of  $\text{var } n_f$  in comparison with M II.

4.1.2. *Cluster field tessellations.*  $\mathbf{E}n_f$  changes only moderately with increasing  $N$ , however,  $\text{var } n_f$  is much greater in the both cluster field tessellations than in PVT (Tab. 3). The pdf's of  $n_f$  have heavier tails caused by the presence of inner cells with low number of faces (tetrahedral and pentahedral inner cells are rather frequent at  $N \lesssim 10$ , say) and by outer cells with very high number of faces. However, in PG tessellations at high  $N$ , the interior of the cluster embedding ball is already a small piece of PVT, the inner cells with low  $n_f$  vanish and simultaneously the proportion of outer cells decreases; consequently, a slow diminution of  $\text{var } n_f$  follows. On the other hand, the growing number of interacting outer cells belonging to different clusters ensure a steady growth of  $\text{var } n_f$  in PS tessellations - see Fig. 4 and note shifts of the nodes in the opposite directions in BePG and BePS tessellations. This behaviour was already observed in the interval  $1 \leq N \leq 30$  and was discussed and



OBRÁZEK 5. Probability density functions of the random dihedral angle  $\theta$  in tessellations generated by Bookstein models at  $a = 0.005$  (full line),  $0.05$  (dotted) and  $0.2$  (dashed).

documented in [14] for PG and PS cluster fields.

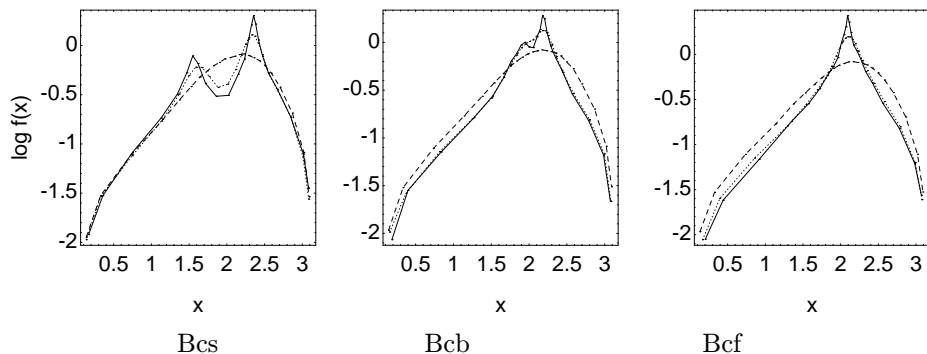
In BePG and BePS tessellations, the lower bound of  $n_f \approx 14$  (without an arrow) relates to  $p = 0.1$ , whereas the upper bound corresponds to PVT; the effect of  $N$  is not substantial (the arrow was omitted accordingly). The maximum values of  $\text{var } n_f$  are attained at  $p = 0.5$  when also CV  $v$  is maximum and they increase with growing cluster cardinality. The mean value  $\mathbf{E}n' = 6$  is obligatory for all primitive (normal) tessellations,  $\text{var } n'$  is higher than in PVT but does not change substantially above  $N = 30$ . In BePS and BePG fields, the fragmentation of the original parent cell boundary *without* implanted cluster by small outer cells of fragmented neighbours is so high that quite extremal values of  $\text{Max } n_f$  can be observed (Tab. 3) and the effect of increasing  $N$  is perceptible even in sections.

#### 4.2. Dihedral and edge angles.

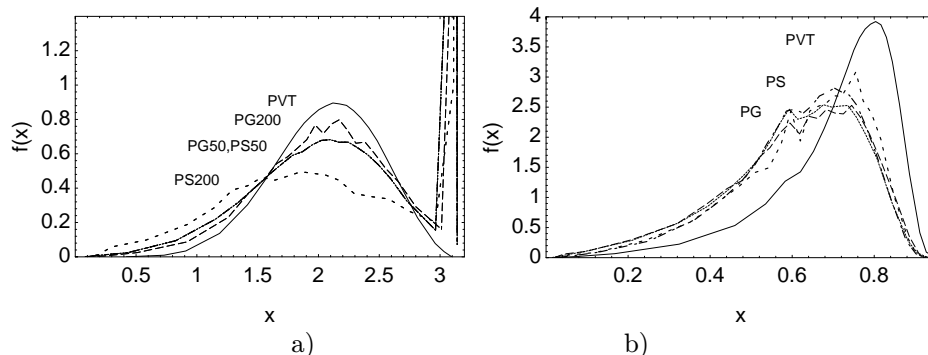
Tab. 4 3D dihedral angles.

	$N$ or $a$	$\mathbf{E}\theta$	$\text{var } \theta$	$\mathbf{E}\Theta$	$\text{var } \Theta$
Bcb	0.05	2.09	0.017	2.09	0.000002
Bcf	0.05	2.09	0.043	2.09	0.0018
Bcs	0.05	2.09	0.112	2.09	0.0043
SSI	-	2.09	0.086	2.09	0.0021
M II	-	2.08	0.122	2.08	0.0065
PVT	-	2.06	0.179	2.07	0.0125
PS	30→200	2.04	0.503→0.563	2.04	0.024←0.027
PG	30→200	2.04→2.05	0.281←0.373	2.04→2.05	0.019←0.024
BeMPVT	50→200	2.05	0.223	2.05	0.017←0.019

4.2.1. *Hard-core and pseudo-hard-core tessellations.* The estimation of dihedral angles confirms the great stability of the tetrakaidecahedral tiling - Fig. 5, Tab. 4: only the narrow interval between the two possible values in the isohedral tiling is covered at  $a = 0.005$  and it becomes wider only slowly. The both Bcf and Bcs tessellations cover considerably wider interval of values. On the other hand, the small differences in pdf's of the edge angle  $\theta'$  (Fig. 6) demonstrate how much of information is lost in induced tessellations.



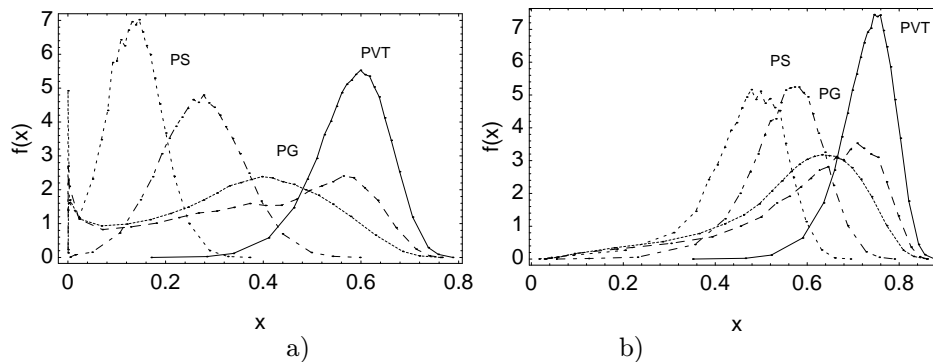
OBRÁZEK 6. Probability density functions of the random dihedral angle  $\theta'$  in the induced 2D tessellations generated by Bookstein models at  $a = 0.005$  (full line),  $0.05$  (dotted) and  $0.2$  (dashed).



OBRÁZEK 7. Probability density functions of the random dihedral angle  $\theta$  (a) and of the 2D shape factor  $f'$  (b) in PVT (full line) and in PG, PS tessellations at  $\delta = 0.05$ . PG:  $N = 50$  (densely dotted), 200 (dashed), PS:  $N = 50$  (dash-dotted), 200 (dotted).

4.2.2. *Cluster field tessellations.* The main change produced in the boundaries of parent cells are new edges created at their intersection with the symmetry planes of closely spaced pairs of daughters; the corresponding dihedral angle is close to the value of  $\pi$  and its frequent occurrence gives rise to the significant secondary mode in the pdf of the random dihedral angles  $\theta, \theta'$  [14] - Fig. 7a.

The dihedral angle  $\theta$  examined here is the *random dihedral angle* - one dihedral angle is selected uniformly at random from each cell. The mean value of  $\theta$  remains nearly unchanged as together with the straight angles mentioned above also two approximately right angles are created. The behaviour of pdf's at  $N \leq 30$  is shown and discussed in [14]. In PG tessellations, the pdf of  $\theta$  approaches that one of PVT at higher values of  $N$ : the inner cells with low face numbers and low dihedral angles gradually vanish. In PS tessellations, the mode systematically shifts to lower values as a manifestation of growing proportion of flat, wedge and pyramidal cells and the increasing fragmentation complexity of parent cells ensures a steady growth of  $\text{var } \theta$ . The distribution of the edge angles - in particular the presence of the secondary mode at  $\theta' \rightarrow \pi$  - in the induced planar tessellations is very similar, hence clusters manifest themselves very clearly this way also in planar sections - Tab. 6.



OBRÁZEK 8. Probability density functions of the mean 3D shape factors  $\mathbf{E}f$  (a) and  $\mathbf{E}g$  (b) in PVT (full lines) and at  $\delta = 0,05$  in PG, PS tessellations. PG:  $N = 50$  (densely dotted), 200 (dashed), PS:  $N = 50$  (dash-dotted), 200 (dotted).

The values for BePS (BePG) tessellations vary between PVT and PS (PG) tessellations.

#### 4.3. Shape factors.

Tab. 5 3D shape factors (the sample size  $\approx 10^6$ ).

	$N$ or $a$	$\mathbf{E}f$	$\min f$	$\mathbf{E}g$	$\min g$
Bcb	0.05	0.788	0.739	0.862	0.828
Bcf	0.05	0.749	0.688	0.856	0.828
Bcs	0.05	0.615	0.552	0.755	0.713
SSI	-	0.686	0.535	0.804	0.691
M II	-	0.639	0.400	0.772	0.580
PVT	-	0.579	0.1	0.728	0.2
PS	30 $\rightarrow$ 200	0.13 $\leftarrow$ 0.32	0.00002	0.46 $\leftarrow$ 0.57	0.0002
PG	30 $\rightarrow$ 200	0.34 $\rightarrow$ 0.39	0.00006	0.55 $\rightarrow$ 0.60	0.01
BeMPVT	50 $\rightarrow$ 200	0.52 $\pm$ 0.01	0.01	0.69 $\pm$ 0.01	0.2

4.3.1. *Hard-core and pseudo-hard-core tessellations.* The shape factors are  $f \propto w^{-3}$  and  $g \propto s^{-2/3}$  in unit isohedral tessellations. Tetrakaidecahedrons create the thinnest tiling with respect to the both surface area  $s$  and mean breadth  $w$ , hence the both shape factors must have the highest values attainable by an isohedral tiling in  $\mathbb{R}^3$ . Note also - Fig. 3b, that the remaining two displaced cubic tessellations become thinner with respect to the both  $s, w$  on growing  $a$ , *i.e.*  $f, g$  increase in certain interval of small values of  $a$ .

The range of shape factors  $f, g$  is relatively narrow in hard- and pseudo-hard-core tessellations and in PVT, no extremely thin or flat cells develop. On the contrary, there is no lower bound on  $f'$  in the corresponding induced tessellations - Tab. 6; highly elongated profiles are created whenever a section plane passes near an edge approximately parallel with it.

4.3.2. *Cluster field tessellations.* A secondary mode near  $f \approx 0$  in the distribution of the shape parameter  $f$  - Fig. 8 - is observed in tessellations generated by cluster fields of both types but it is insignificant and occurs at higher values of  $N$  in tessellation produced by spherical fields. It is produced by rod-like cells of small volume  $v$  and

appreciable mean breadth  $w$ . A comparable fraction of plate-like cells would create a similar mode near zero in the distribution of the shape factor  $g$ , but this distribution is the only one which is strictly unimodal; hence plate-like cells must be rather rare.

Tab. 6 2D shape factor and edge angles (the sample size  $\approx 10^6$ ).

	$N$ or $a$	$\mathbf{E}f'$	$\min f'$	$\mathbf{E}\theta'$	$\text{var } \theta'$
Bcb	0.05	0.808	0.004	2.00	0.021
Bcf	0.05	0.808	0.003	2.02	0.020
Bcs	0.05	0.712	0.002	2.01	0.030
SSI	-	0.760	0.002	2.01	0.25
M II	-	0.739	0.002	2.01	0.29
PVT	-	0.579	0.003	2.000	0.349
PS	30→200	0.6	0.001	2.00	0.513←0.576
PG	30→200	0.62	$\approx 0$	1.96→1.97	0.584←0.61
BeMPVT	50→200	0.69±0.01	0.003	1.99	0.39→0.41
BePS	30→99				
BePG	30→200				

A distinct bimodality was observed also in the distribution of planar the shape factor  $f'$ , even in PVT [5]. The position of the secondary mode is rather stable. Its probable cause is the abundant presence of triangular profiles formed whenever a section plane hits a cell near its vertex (the mode value  $f' \approx 0.6$  is appropriate to an equilateral triangle) and it is more pronounced in PG and PS tessellations - Fig. 7. The values for BePS (BePG) tessellations vary between PVT and PS (PG) tessellations.

## 5. SUMMARY

In the examined sequence of hard- and pseudo-hard-core tessellations, a gradual passage is accomplished from a regularity of point arrangement in translation lattices to a complete independence of points in PPP. This passage is reflected by the dual representation of point patterns through the properties of Voronoi cells, namely as a passage from dense (in the sense of inscribed sphere volumes) and thin (with respect to cell boundary properties) tilings to PVT. Its main features are an increase (not always monotone) of the values and ranges of the face, edge and vertex numbers and the loss of equiaxiality (decreasing shape factors and a continuous range of dihedral angles spanning finally the whole interval  $(0, \pi)$ ).

At small values of cluster size  $\delta$  and growing cluster cardinality  $N$ , globular cluster fields gradually realize a local point concentration. At sufficiently high  $N$ , the points are compressed within the cluster embedding balls separated by large pointless regions. The majority of them generates inner cells gradually approaching a piece of PVT, which explains the "left arrows" in the rows of the tables describing PG tessellations. Only the points lying in the vicinity of the ball boundary generate large outer wedge-, rod- and plate-like cells filling up the vast space between individual clusters. These cells forming quasi-spherical bundles resemble cells of spherical clusters and their properties differ from those of PVT - they have lower values of  $\mathbf{E}\theta$  and of shape factors and cover wider ranges of  $\theta$  and  $n_f$ . Their effect on the mean values gradually fades out with growing  $N$  in PG cluster fields and the direction of their gradual development - symbolized by "right arrows" in the corresponding table rows - must be examined in the PS fields only. Unfortunately even in such fields, small PVT-islands are formed by clusters innate to PPP at high values of  $N$ .

In the Bernoulli mixtures and Bernoulli cluster fields, the above described mixing of various types of Voronoi cells can be better controlled than in pure PG and PS fields.

Due to their scale independence, shape properties are very suitable for an exploratory analysis of point patterns as well as of natural tessellations.

#### REFERENCE

- [1] K. Bodlák, P. Ponížil, I. Saxl: *3D Voronoi tessellation generated by Strauss process*. Proc. Summer school "Robust 2000" (this issue).
- [2] P. Engel: *Geometric crystallography*. In: Handbook of Convex Geometry (P. M. Gruber, J. M. Wills, eds.). North-Holland, Amsterdam 1993, pp. 989-1022.
- [3] E. С. Федоров: Начала учения о фигурах. Изд. Акад. наук, Ленинград 1953.
- [4] L. Fejes Tóth: *Lagerungen in der Ebene auf der Kugel und im Raum*. Springer-Verlag, Berlin 1953.
- [5] M. Goldberg: *Several new space-filling polyhedra*. Geometriae Dedicata **5** (1976), 517-523.
- [6] M. Goldberg: *Convex polyhedral space-fillers of more than twelve faces*. Geometriae Dedicata **8** (1979), 491-500.
- [7] B. Grünbaum, G. C. Shephard: *Tilings with congruent tiles*. Bull. Amer. Math. Soc. **3** (1980), 951-973.
- [8] Lorz U, Hahn U: *Geometric characteristics of random spatial Voronoi tessellations and planar sections*. Preprint 93-05. Freiberg: Bergakademie Freiberg, 1993.
- [9] Minkowski H: *Allgemeine Lehrsätze über die konvexen Polyeder*. Nachr. Ges. Wiss. Göttingen, Math-Phys Kl (1897), 198-219.
- [10] Okabe A., Boots B., Sugihara K.: *Spatial Tessellations*. J. Wiley & Sons, Chichester 1992.
- [11] P. Ponížil and I. Saxl: *Properties of 3D Poisson hard-core and pseudo-hard-core fields II. Voronoi tessellations*. Proc. S<sup>4</sup>G, Int. Conf. on Stereology, Spatial Statistics and Stochastic Geometry, (V. Beneš, J. Janáček and I. Saxl, eds.), JČMF, Praha, pp. 227-239 (1999). See also a substantial part of all data and a summarizing paper on the Internet address: <http://fyzika.ft.utb.cz/voronoi/>.
- [12] I. Saxl and P. Ponížil: *3D Voronoi tessellations of cluster fields*. Acta Stereol. **17** (1998), 237-246.
- [13] I. Saxl and P. Ponížil: *3D Voronoi tessellations generated by Poisson and lattice cluster fields*. Acta Stereol. **17** (1998), 247-252.
- [14] Saxl I, Ponížil P.: *Shapes of Voronoi polytopes*. In: Proc. Int. Conf. "Prague Stochastics '98", (M. Hušková, P. Lachout, J.Á. Víšek, eds.). JČMF, Praha 1998, 505-10.
- [15] Saxl I.: *Analýza náhodných bodových vzdáleností a Voronoiovy teselace systémů*. In: Robust'98 (J. Antoch, G. Dohnal, eds.), JČMF, Praha 1998, 161-178.
- [16] I. Saxl, P. Ponížil: *Bernoulli cluster fields: Voronoi tessellations*. Submitted to *Appl. Math.*
- [17] E. Schulte: *Tilings*. In: Handbook of Convex Geometry (P. M. Gruber, J. M. Wills, eds.). North-Holland, Amsterdam 1993, pp. 901-926.
- [18] D. Stoyan, W. S. Kendall and J. Mecke: *Stochastic Geometry and its Applications*. J. Wiley & Sons, New York (1995).
- [19] D. Stoyan, H. Stoyan: *Fractals, Random Shapes and Point Fields*. J. Wiley & Sons, Chichester, 1994.
- [20] G. F. Voronoi: *Nouvelles applications des paramètres continus à la théorie des formes quadratiques. Deuxième Mémoire, Recherche sur les parallélogrammes primitifs*. J. Reine Angew. Math. **134**, (1908), 198-287.

CZECH ACADEMY OF SCIENCES, MATHEMATICAL INSTITUTE, ŽITNÁ 25, CZ-110 00 PRAHA 2, CZECH REPUBLIC

E-MAIL: saxl@math.cas.cz